

Dynamic electrowetting of sessile drops on soft surfaces

Ranabir Dey¹, Ashish Daga¹, Sunando DasGupta^{2,3}, Suman Chakraborty^{1,3*}

¹*Department of Mechanical Engineering, Indian Institute of Technology Kharagpur, Kharagpur- 721 302, West Bengal, India.*

²*Department of Chemical Engineering, Indian Institute of Technology Kharagpur, Kharagpur- 721 302, West Bengal, India.*

³*Advanced Technology Development Centre, Indian Institute of Technology Kharagpur, Kharagpur- 721 302, West Bengal, India.*

ABSTRACT

Electrically-mediated dynamic wetting behaviour of sessile liquid drops on dielectric films is governed by the combined interplay of the wetting line friction and the internal viscous dissipation. We show here that such classical description of the electrospredding phenomenon, as prevalent in the contemporary literature, fails to address the electro-capillarity induced dynamic wetting of sessile drops on soft dielectrics. We first delineate the temporal variations of the macroscopic dynamic contact angle, and the contact radius, during electrowetting on rheologically tunable soft surfaces, at different applied electric potentials; subsequently, we prove through a scaling analysis, and an energy conservation approach, that the dielectric elasticity dependent, microscale elastocapillary deformation of the soft substrate, near the three-phase contact line, plays the integral role in dictating the macroscopic electrowetting behaviour. Interestingly, under such electro-elastocapillary phenomenon on soft dielectrics, the variations of the contact radius and the dynamic contact angle follow universal trends, stemming from the combined influence of the wetting line friction and the viscoelastic dissipation. This work will be instrumental in paving the way towards the realization of yet unexplored paradigm of electro-elastocapillary applications, especially in the bio-physical context.

* Corresponding author, E-mail: suman@mech.iitkgp.ernet.in

The electrically-tunable partial wetting of a conductive liquid droplet on a dielectric layer, classically termed as electrowetting-on-dielectric (EWOD) [1–4], is one of the principal modalities of discrete droplet-handling. Electrowetting-based platforms for droplet manipulations (digital microfluidic platforms) have revolutionized microscale thermal management, microscale mixing, microscale chemical reactors, and bio-medical engineering, especially rapid diagnostic tests, by circumventing the inherent limitations of continuous flow and droplet microfluidics [5–7]. Furthermore, the other state-of-the-art applications of electrowetting, and subsequent dewetting, also include variable focus-lenses [2,4], electronic displays/e-papers [2,4], control of droplet morphology over functional substrates [8–11], and control of interfaces between immiscible electrolyte solutions [12]. Such growing ubiquitousness of the electrowetting phenomenon necessitates a fresh look at certain unaddressed aspects of the involved interfacial dynamics, which may eventually translate into further process-controlling methodologies.

On application of an external electric potential to a conductive-droplet-and-dielectric system (see Fig.1 (a)), the accumulation of charges at the solid-liquid interface leads to substantial reduction in the associated interfacial energy [1–4]. Such electrically-induced alteration in the capillarity of the system initiates the spreading of the droplet on the dielectric layer. The associated driving capillary force is given by [13–15]: $F = \gamma [\cos \theta_{eq}(V) - \cos \theta_d(t)]$, where γ is the liquid surface tension, $\theta_{eq}(V)$ is the final equilibrium contact angle attained by the droplet under the applied electric potential V , and $\theta_d(t)$ is the macroscopic dynamic contact angle during the electrowetting process. During the electrowetting on rigid substrates, the expended capillary free energy- Fv_{cl} , where v_{cl} is the contact line velocity, is consumed by the viscous dissipation due to the internal hydrodynamics of the spreading droplet, in conjunction with the molecular energy dissipation (or contact line dissipation) in the immediate vicinity of the three-phase contact line (TPCL) [13,14,16,17]. This dynamic energy balance actually controls the rate of the droplet spreading, and dictates the nature of variation of θ_d with v_{cl} , during electrowetting. However, during the initial wetting stage (i.e. when a droplet just contacts the dielectric surface), preceding the conventional electrowetting paradigm, the wetting dynamics is solely dominated by the balance between capillary and inertial forces [18,19]; and it must be noted here that this regime is outside the purview of the present discourse. The aforementioned theoretical framework [13,14,16,17], for the conventional dynamic electrospreeding, fails to capture any possible alterations in the electrically-mediated dynamic wetting behaviour due

to changes in the solid-liquid interfacial dynamics, stemming from the variations in dielectric mechanical properties in general, and dielectric elasticity in specific.

In general, a sessile droplet resting on a soft substrate results in the deformation of the substrate near the TPCL, with a locally triangular shape (a ‘cusp’) at the contact line [20]. This substrate deformation is a manifestation of the elastocapillary response of the soft substrate to the interfacial capillary interactions, due to the presence of the droplet [20–25]. The characteristic length-scale (γ/E), for this substrate deformation, is dependent on the liquid surface tension (γ) and the Young’s modulus of the substrate (E) [20,23–26]. It goes without saying that such microscopic deformation of the soft substrate, which leads to the formation of the ‘wetting ridge’ near the TPCL (see Fig. 1(c), Fig. 1(d)), unilaterally alters the macroscopic spreading/dewetting dynamics of liquid drops [27–32]. Taking cognizance of such altered contact line dynamics on soft substrates, *the question that we want to address here is how do such interfacial elastocapillary interactions alter the electrowetting behaviour of sessile liquid drops on soft dielectrics?*

In this letter, we show the electrically induced dynamic wetting behaviour of conductive sessile droplets on rheologically tunable soft dielectric films. We first experimentally delineate the temporal variations in macroscopic dynamic contact angle, and contact radius, of sessile droplets, during the wetting process on dielectrics with decreasing elasticity (i.e. increasing ‘softness’), at different magnitudes of the applied electric potential. Thereafter, we propose a theoretical framework, commensurate with the yet unexplored paradigm of such electro-elastocapillary interactions, to address the observed electrically-mediated dynamic wetting behaviour on the softer films.

For the present experiments, dielectric films of varying elasticity are prepared from Sylgard 184 (Dow Corning, USA; dielectric constant, $\epsilon_r = 2.65$)- a two part, thermocurable, cross-linked, Polydimethylsiloxane (PDMS) based elastomer. The prepolymer is prepared by mixing the base and curing agent in the weight ratios of 10:1, 30:1 and 50:1. The degassed prepolymer is then spin-coated (spin coater: Süss MicroTec, Germany) on transparent Indium Tin Oxide (ITO) coated glass slides (Sigma-Aldrich; surface resistivity 70-100 Ω/sq), followed by subsequent overnight curing at 95 °C. Bulk rheometry tests reveal that the Young’s modulus (E) of the differently cross-linked Sylgard 184 films decreases from 1.5 MPa to 0.02 MPa, with increasing base-to-cross-linker ratio, which is in accordance with the trend established in the literature [33,34]. The root mean square roughness (r_{RMS}) of the different film surfaces, as measured by atomic force microscopy, do not exceed 0.303 nm.

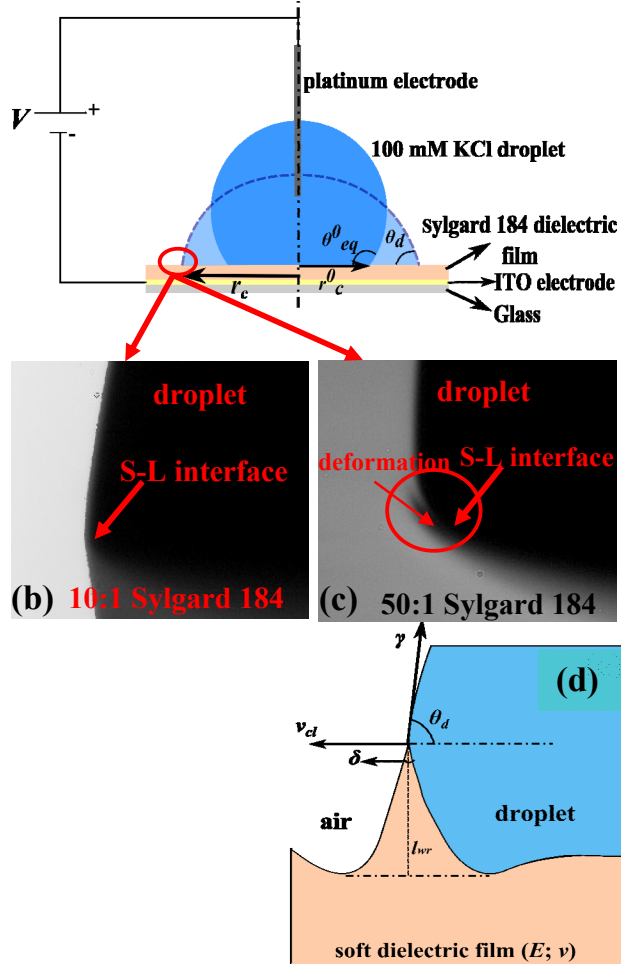


FIG. 1 (a) The schematic of the droplet-and-dielectric system used for investigating the dynamic electrowetting behaviour of sessile drops on soft surfaces. (b) A magnified image (blow up) of the advancing droplet meniscus, near the TPCL, on the rigid 10:1 Sylgard 184 dielectric film, (c) on the 50:1 Sylgard 184 dielectric film. On the rigid substrate, the droplet and the dielectric film form a sharp solid-liquid (S-L) interface. Interestingly, on the softer dielectric film, the S-L interface exhibits an apparent deformation of the substrate close to the TPCL. For the soft dielectric films (i.e. 30:1 and 50:1 Sylgard 184 films), the length scale for such deformation, $l_{wr} \sim \gamma/E \sim O(10^{-6} \text{ m})$ (d) Schematic showing the elastocapillary deformation of the soft dielectric films, culminating in the formation of the wetting ridge at the TPCL, during the electrowetting induced droplet spreading on soft dielectrics. The local modification of the contact angle due to the substrate deformation is neglected on a macroscopic scale [27-30, 32].

Moreover, the Sylgard 184 films of varying elasticity are also characterised by evaluating the equilibrium contact angle (θ_{eq}^0), the macroscopic advancing and receding contact angles (θ_a^0 / θ_r^0) of aqueous 100 mM KCl solution droplets (Milli-Q ultrapure water; Millipore India Pvt. Ltd.) on the films, without considering any electrical effects (see Table 1). The electrowetting experiments are performed with the sessile droplets of aqueous 100 mM KCl solution ($\gamma = 72.75 \times 10^{-3} \text{ N/m}$; viscosity, $\mu = 1.002 \times 10^{-3} \text{ Pa} \cdot \text{s}$; electrical

conductivity, $\sigma = 1.215 \text{ S/m}$). A sessile droplet of volume $5 \pm 1 \mu\text{l}$ (initial droplet contact radius- $r_c^0 = 1.28 \text{ mm}$, is independent of substrate elasticity; only 2.45% deviation is observed across different substrates) is dispensed onto the dielectric layer, with a definite value of E , by a calibrated microsyringe. The ensuing spreading dynamics, on application of a DC electric potential (V) (Keithley instruments: 0-1 KV) between the platinum wire electrode immersed in the droplet and the ITO electrode (see Fig. 1(a)), is recorded at 2000 fps by a high speed camera (Phantom v641) fitted with a macro zoom lens (Navitar Macro zoom, 18-108 mm F/2.5; image resolution- 640x480 pixels x24 bits) [35]. In a further attempt to resolve the deformation of the softer substrates near the TPCL, during the spreading process, high speed magnified images are also recorded with the Phantom v641 camera, integrated with a microscopic lens (Infiniprobe TS-160 with 16x objective; image resolution- 1918x1078 pixels x24 bits) (see Fig. 1(b) and Fig. 1(c)). For each of the three different dielectric films, identical experiments are performed at different voltages ranging between 100 V and 160 V. The variations in dynamic contact angle, and contact radius, are evaluated from subsequent image processing by using ImageJ software [36]; while the involved data analysis is performed with in-house MATLAB codes (v. R2012a, The MathWorks, Inc., USA).

Table 1: Young's modulus, thickness of differently cross-linked Sylgard 184 dielectric layers; equilibrium contact angles, advancing and receding contact angles (at zero applied potential), of 100 mM aqueous KCl solution on different PDMS films

	PDMS 10:1	PDMS 30:1	PDMS 50:1
$E \text{ (MPa)}$ [33,34]	1.5	0.06	0.02
$h \text{ (}\mu\text{m)}$	9.65	11.34	7.02
$\theta_{eq}^0 \text{ (}^\circ\text{)}$	109.24 ± 0.05	110.07 ± 3	116.03 ± 2.41
$\theta_a^0 / \theta_r^0 \text{ (}^\circ\text{)}$	115.6/102.7	121.6/39.13	126.95/29.06

The temporal variations of the dynamic contact angle (θ_d) and the contact radius (r_c), during the wetting process under different magnitudes of the applied electric potential (V), on dielectrics of varying elasticity, are shown in Fig. 2(a) and Fig. 2(b) respectively. Here, $\bar{\theta}_d = \theta_d / \theta_{eq}^0$ and $\bar{r}_c = r_c / r_c^0$. On application of the electric potential, the rate of

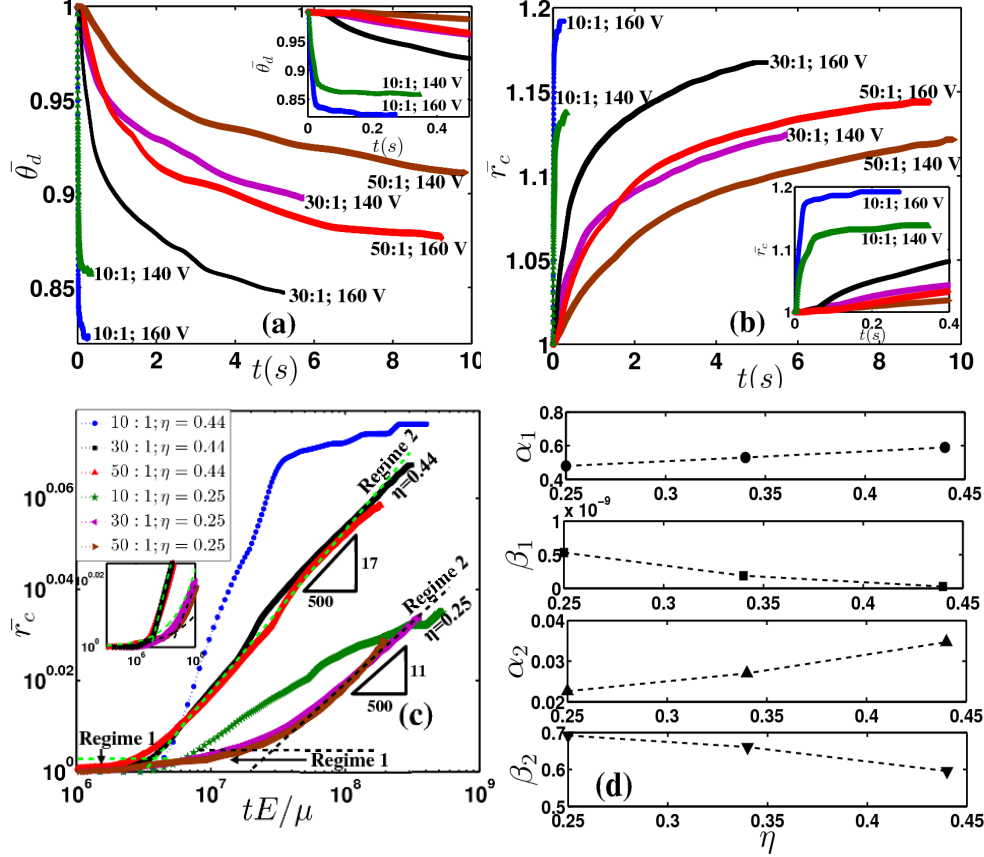


FIG. 2 Electrically-induced temporal variations of (a) the non-dimensional macroscopic dynamic contact angle ($\bar{\theta}_d$), (b) the non-dimensional contact radius (\bar{r}_c), on dielectric (Sylgard 184) films of varying elasticity ($E \sim 1.5 - 0.02$ MPa), at different magnitudes of the applied electric potential (140 V and 160 V). The errors involved in the measurement of $\bar{\theta}_d$ and \bar{r}_c are $\sigma_{ca} = \pm 0.031$ and $\sigma_{cr} = \pm 0.062$ respectively. (c) Collapse of the \bar{r}_c vs. t data sets, for the softer dielectric films, into distinct master curves, one corresponding to each value of the non-dimensional electrowetting number η (shown here for $\eta = 0.25$ and 0.44 , for sake of clarity; for the data reduction corresponding to 140 V, i.e. $\eta = 0.34$, see [35]), on rescaling with a liquid viscosity and substrate elasticity dependent time scale (μ/E). The master curves exhibit two distinct regimes of power-law dependencies in the reduced time (see inset for better clarity), where the values of the prefactor (β_i) and the power-law exponent (α_i), for both the regimes ($i = 1, 2$), are functions of η , as shown in (d). The electrowetting behaviour on the rigid 10:1 film does not conform to the master curves.

decrease of the dynamic contact angle is faster on the substrate with greater elasticity, i.e. $\bar{\theta}_d$ decreases faster on the 10:1 Sylgard 184 dielectric film as compared to that on the 50:1 Sylgard 184 dielectric film (see Fig. 2(a)). However, it is the variation of the contact radius that unambiguously shows that at a definite magnitude of V , the electrically-induced droplet spreading rate appreciably decreases, and hence, the total spreading time consequently increases, with increasing dielectric softness (i.e. decreasing E ; see Fig. 2(b)). Furthermore,

under a specific magnitude of V , the final static value of the contact radius progressively decreases, and the corresponding measured equilibrium contact angle value increases, with decreasing magnitude of E (see Fig 2(a) and Fig. 2(b)). In essence, the rate and extent of electrowetting, at a definite magnitude of V , decreases with decreasing dielectric elasticity. However, on a particular dielectric film, the rate and extent of electrowetting increase with the increasing magnitude of the applied electric potential, as intuitively expected (see Fig. 2(a) and Fig. 2(b)).

From dimensional analysis it is evaluated that $\bar{r}_c = f\left(\frac{t}{\mu/E}; \eta\right)$, where $f(\)$ is

some function and $\eta = \epsilon_r \epsilon_0 V^2 / 2h\gamma$ is the (non-dimensional) electrowetting number, which represents the ratio of the electrically-induced change in the solid-liquid interfacial energy to the liquid surface tension [1]. On non-dimensionalizing the droplet electrospredding data for dielectric films of varying elasticity (i.e. the \bar{r}_c vs. t data sets as shown in Fig. 2(b)) with this particular time scale (μ/E), the data sets for the softer dielectric films (i.e. the 30:1 and 50:1 Sylgard 184 films) collapse into distinct master curves, one corresponding to a definite value of η (see Fig. 2(c)). However, the droplet spreading curve for the rigid 10:1 dielectric film [37], at a definite value of η , deviates from the corresponding master curve. Alternatively, the rescaling of the experimental data sets by an inertia and substrate elasticity dependent time scale ($\sqrt{\rho(r_c^0)^2/E}$; where ρ is the liquid density), which also stems from the dimensional analysis, fails to reduce these into master curves. Hence, it can be now unequivocally concluded that the dynamic electrowetting phenomenon on a dielectric is intrinsically dominated by the combined effects of the *elasticity of the dielectric and liquid viscosity*, and is not generally independent of the dielectric mechanical properties as prevalent in the contemporary literature [13–17]. Moreover, the characteristic electrowetting time scale (μ/E) also implies that smaller the Young's modulus of the dielectric, greater is the characteristic time for the spreading process, which is in accordance with the aforementioned experimental results. Furthermore, this particular time scale can be thought of as the product of the viscocapillary time scale ($\mu r_c^0 / \gamma$), which is considered for droplet spreading dominated by the balance between viscosity and capillarity of the system [18], and a factor ($\frac{\gamma/E}{r_c^0}$), which represents the non-dimensional length scale for the capillarity-induced

deformation of the soft substrate [20,23–26]. This further highlights the fact that the dynamic electrowetting behaviour is in general influenced by the elastocapillarity of the droplet and dielectric system, which cannot be neglected *a priori*. Now, the log-log plot in Fig. 2(c) also reveals that the master curves, for electrospreeding on soft substrates, exhibit two distinct regimes of temporal dependencies (i.e. two different functional forms for $f(\cdot)$): in *Regime 1*, $f(\cdot)$ corresponds to the form $\bar{r}_c = 1 + \beta_1(\eta)[tE/\mu]^{\alpha_1(\eta)}$; while in *Regime 2*, $f(\cdot)$ has the more conventional power-law form $\bar{r}_c = \beta_2(\eta)[tE/\mu]^{\alpha_2(\eta)}$. Here, the prefactor $\beta_i(\eta)$ and the power-law exponent $\alpha_i(\eta)$ ($i=1$ for *Regime 1* and $i=2$ for *Regime 2*) are functions of η (see Fig. 2(d)). The values of $\alpha_i(\eta)$ and $\beta_i(\eta)$, as well as Fig. 2(c) itself, clearly indicate that the temporal variation of \bar{r}_c in *Regime 2* becomes steeper, while the extent of *Regime 1* becomes smaller, with increasing magnitude of η . To comprehend the underlying physical phenomena, culminating in such markedly different electrowetting behaviour on soft dielectrics, it is beneficial to address the droplet spreading problem through an energy conservation approach, which first necessitates the evaluation of the θ_d dependence on the contact line velocity ($v_{cl} = \dot{r}_c$).

On non-dimensionalizing v_{cl} with a characteristic velocity scale ($v_o = \frac{r_c^0}{\mu/E}$),

commensurate with the substrate elasticity dependent electrowetting time scale, the dynamic contact angle variations with the contact line velocity, on the softer substrates, also collapse into master curves, one for a definite value of η (see Fig. 3(a); here,

$$\bar{v}_{cl} = \frac{v_{cl}}{v_o} = \frac{\mu v_{cl}}{r_c^0 E} = \frac{\mu v_{cl}}{\gamma} \times \frac{\gamma/E}{r_c^0}. \text{ This further proves that during electrowetting on soft}$$

substrates, θ_d dependence on v_{cl} is dictated by the elasticity dependent interfacial elastocapillary phenomenon, unlike the θ_d vs. v_{cl} relationship for electrically-mediated dynamic wetting on rigid substrates [13–17]. On a rigid dielectric substrate (i.e. the 10:1 Sylgard 184 film), the expenditure of the capillary free energy (Fv_{cl}) associated with the spreading, in the range of higher contact line speeds, is predominantly balanced by the molecular energy dissipation, in the immediate vicinity of the TPCL, as elucidated by the linear Molecular Kinetic Theory (MKT) [38,39]; accordingly, the θ_d variation, for higher

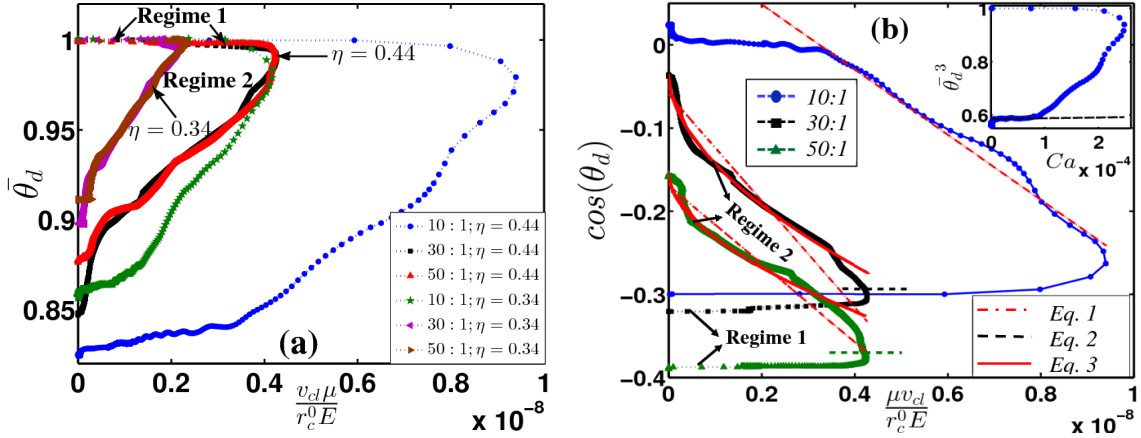


FIG. 3 (a) Collapse of the non-dimensional macroscopic dynamic contact angle ($\bar{\theta}_d$) vs. the contact line velocity (v_{cl}) data sets, for the softer dielectric films, into master curves, one for a definite value of η (shown here for $\eta = 0.34$ and 0.44), on reducing v_{cl} with a characteristic velocity scale ($r_c^0 E / \mu$). (b) Description of the electrically-mediated variation of macroscopic dynamic contact angle (θ_d), with the reduced velocity ($v_{cl}\mu / r_c^0 E$), through an energy conservation approach for $\eta = 0.44$. The electrowetting behavior on the rigid 10:1 film is satisfactorily addressed by the balance between the capillary free energy and the wetting line friction (Eq. 1) in the range of higher values of v_{cl} ; while in the range of lower values of v_{cl} , θ_d variation is well accounted for by the pertinent hydrodynamic description (Eq. 2), as shown in the inset through the $\bar{\theta}_d^3$ vs. Ca relationship. However, the variation of θ_d with the reduced velocity, for the softer dielectric films, is governed by the combined influence of the wetting line friction, and the viscoelastic energy dissipation due to the elastocapillary deformation of the soft substrate near the TPCL (Eq. 3) (hence, the dependence of the characteristic time and velocity scales, for the soft substrates, on μ and E); viscous dissipation plays no role for the softer substrates. The measured and fitted values of different parameters involved in Eqs. 1, 2 and 3 are listed in [35]. For the fitting procedure, a robust non-linear least squares method is implemented here.

values of v_{cl} , is coherently addressed by the following relationship stemming from the energy conservation principle (see Fig. 3(b)):

$$\cos \theta_d = \cos \theta_{eq}(\eta) - \frac{\zeta v_o}{\gamma} \bar{v}_{cl} \quad (1)$$

where ζ is the co-efficient of wetting line friction which, on combining Eyring's formula for liquid viscosity with the linearized MKT theory, can be expressed as [35]:

$$\zeta = \mu \left(\frac{v_l}{\lambda^3} \right) \exp \left(\frac{\gamma \lambda^2 (1 + \cos \theta_{eq}) - 2 d_m^2 \gamma}{k_B T} \right). \text{ Here, } k_B \text{ is the Boltzmann constant, } T \text{ is the}$$

absolute room temperature, λ is the distance between liquid molecule adsorption sites on the dielectric surface, v_l is the unit volume of flow of the liquid, which for simple liquids

corresponds to the molecular volume- $v_m = d_m^3 = \left(\frac{M_w}{N_A \rho} \right)$, where d_m is the molecular diameter ($\sim 3.103 \times 10^{-10}$ m for the test liquid), M_w is the liquid molecular weight and N_A is the Avogadro number. On the other hand, the θ_d variation, in the range of smaller values of v_{cl} (i.e. in the later stages of electrowetting on the rigid film), conforms to the hydrodynamic description, stemming from the matching of the Stokes flow solution in the quasi-static macroscopic region to that in the mesoscopic viscocapillary region of the droplet interface near the TPCL, for the advancing meniscus problem [38–40](see inset in Fig. 3(b)):

$$\theta_d^3 = \theta_{d,m}^3 + 9Ca \ln \left(\phi \frac{L}{l} \right) \quad (2)$$

Here, $\theta_{d,m}$ is the microscopic dynamic contact angle, $Ca = \frac{\mu v_{cl}}{\gamma} = \text{Capillary number}$, L is a macroscopic length comparable to the droplet size ($\sim r_c^0$), l is a microscopic cut-off length beyond which the hydrodynamic framework collapses, and ϕ is a problem specific numerical constant [41]. Interestingly, the aforementioned description of the electrowetting dynamics, on the rigid 10:1 Sylgard 184 film, fails to capture the electrically-induced wetting behaviour on the softer films (see Fig. 3(b)). On the soft surfaces, the wetting ridge (see Fig. 1(c), Fig. 1(d) and Fig. 1(e)), formed due to the elastocapillary deformation of the substrate, also moves along with the advancing contact line. The associated rate of expenditure, per unit length of the triple line, of the deformation/strain energy in ‘pulling up’ this wetting ridge is given as

$$[27]: \dot{W} \approx \frac{2\gamma^2(1-\nu^2)}{\pi E \delta} v_{cl} (\sim (l_{wr} \gamma v_{cl})/r_c), \text{ where } l_{wr} \sim \gamma/E \text{ is the length scale for the height of}$$

the wetting ridge), where ν is the Poisson’s ratio ($\nu = 0.5$ for incompressible materials), and δ is the (sub-nanometric) length of the region, about the TPCL, within which the linear elasticity theory no longer holds true. Now, due to the viscoelastic nature of soft solids in general (specifically elastomers, like Sylgard 184), a rate-dependent fraction, $\Delta = (v_{cl}/v_c)^n$, of the strain energy (\dot{W}) is always dissipated, while the rest is restituted, as the soft solid relaxes after the passage of the liquid front and the concomitant displacement of the wetting ridge to a new position [30,32]. Here, v_c is a constant characteristic velocity, which is taken here as v_o , and n is a power-law index reflective of the surface damping properties. So, on incorporating this viscoelastic dissipation, the dynamic energy balance between the rate of

expenditure of the capillary free energy and the total rate of energy dissipation, during electrowetting, can be written as:

$$\cos \theta_d = \cos \theta_{eq}(\eta) - \frac{\zeta v_o}{\gamma} \bar{v}_{cl} - \frac{3\gamma}{2\pi E\delta} (\bar{v}_{cl})^n \quad (3)$$

This equation nicely captures the electrically-induced variation of θ_d with the reduced contact line velocity, on a general soft dielectric, at any given value of η (see Fig. 3(b)). For

this ‘master equation’, the non-dimensional co-efficients- $\frac{\zeta v_o}{\gamma}$ (contribution of the contact

line friction) $\sim (1.019 \pm 0.0732) \times 10^4$, and $\frac{3\gamma}{2\pi E\delta}$ (contribution of the viscoelastic

dissipation) $\sim (8.4921 \pm 0.7134) \times 10^3$, while $n \sim 0.5518 \pm 0.0085$. It must be noted here that

while the ratio of the rate of contact line dissipation to the rate of viscoelastic energy dissipation is $\sim O(1)$, the ratio of viscous dissipation (due to internal hydrodynamics) to the

viscoelastic dissipation is $\sim O(10^{-2} - 10^{-1})$; consequently, viscous dissipation is neglected here [42]. Moreover, we also confirmed that the pertinent hydrodynamic description (i.e. Eq.

2) fails to significantly address the θ_d vs. v_{cl} relationship on soft substrates. Hence, the combined contact line and viscoelastic energy dissipation mechanisms intrinsically control

the electrowetting behaviour of sessile drops on soft dielectrics, and it is this behavioural regime that constitutes the previously mentioned *Regime 2* (see Fig. 3(b)). While *Regime 1*

simply represents the regime over which the contact line velocity instantaneously accelerates from zero to its maximum magnitude with no substantial reduction in θ_d , on application of

V , before the dissipation mechanisms ‘kick in’ (see Fig. 3(b)). *Regime 1* is usually never depicted in electrowetting analysis [13,14,16,17], and *Regime 2* is considered as the actual

‘electrowetting regime’.

We conclude here that the electrically-mediated dynamic wetting behaviour on soft substrates is dictated by the combined interplay of the wetting line friction, as described by the Eyring’s formula for viscosity and the linearized MKT theory, and the viscoelastic energy dissipation due to the advancing contact-line ridge formed by the elastocapillary deformation of soft substrates, as captured by linear elasticity theory. The increasing magnitude of this additional viscoelastic dissipation, with decreasing E , impedes the electrospreeding rate on softer dielectrics, at a definite magnitude of the applied electric potential, and in essence, acts as the primary rate-controlling factor. Under such electro-

elastocapillary phenomenon, the spreading radius in general follows a power-law dependence in time, of the form- $\bar{r}_c = \beta(\eta)[tE/\mu]^{\alpha(\eta)}$, while the reduction of the macroscopic dynamic contact angle generally conforms to an explicit function of the reduced contact line velocity ($\bar{v}_{cl} = \frac{\mu v_{cl}}{r_c^0 E}$), of the form- $\cos \theta_d = \cos \theta_{eq}(\eta) - A\bar{v}_{cl} - B(\bar{v}_{cl})^{0.55}$, where A and B are numerical constants. Such dynamic electrowetting behaviour on soft surfaces is distinctly different from the classical electro-capillarity induced wetting behaviour on rigid dielectric films, which is independent of any viscoelastic phenomenon stemming from the rheological behaviour of the dielectric. Hence, the classical electrospreeding on rigid dielectrics do not adhere to the ‘master equations’, and consequently the ‘master curves’, elucidating the same on the softer dielectric films. In reality, for hard substrates, the length scale for substrate deformation, $\gamma/E \sim O(10^{-9} \text{ m})$, is comparable to molecular dimensions; hence, the description of the associated elastocapillary response of the substrate not only requires a completely different approach [25,43], but also primarily fails to perceptibly alter the wetting behaviour of millimetre-sized droplets, as encountered in vast majority of electrowetting applications. The present study on the dynamic electrowetting behaviour of sessile drops on soft surfaces can be the genesis of an entirely new branch of electrowetting applications involving soft surfaces- like development of soft lenses mimicking the functioning of the human eye, and flexible electronic displays with soft films for better configurability and manoeuvrability; and more importantly, applications involving biological surfaces (which primarily involve soft tissues)- like control of spreading in bio-physical processes.

-
- [1] J. Berthier, Microdrops and digital microfluidics, William Andrew, Norwich, NY, USA (2008).
 - [2] F. Mugele and J.-C. Baret, J. Phys. Condens. Matter **17**, R705 (2005).
 - [3] L. Y. Yeo and H.-C. Chang, Mod. Phys. Lett. **19 (12)**, 549 (2005).
 - [4] R. Shama, D. Andelman, B. Berge, and R. Hayes, Soft Matter **4**, 38 (2008).
 - [5] P. Y. Paik, K. Chakrabarty and V. K. Pamula, IEEE Design and Test of Computers, 372 (2008).
 - [6] P. Paik, V. K. Pamula, and R. B. Fair, Lab Chip **3**, 253 (2003).
 - [7] K. Choi, A. H. C. Ng, R. Fobel, and A. R. Wheeler, Annu. Rev. Anal. Chem. **5**, 413 (2012).

- [8] V. Bahadur and S. V Garimella, *Langmuir* **23**, 4918 (2007).
- [9] T. N. Krupenkin, J. A. Taylor, E. N. Wang, P. Kolodner, M. Hodes, and T. R. Salamon, *Langmuir* **23**, 9128 (2007).
- [10] V. Bahadur and S. V Garimella, *Langmuir* **24**, 8338 (2008).
- [11] G. Manukyan, J. M. Oh, D. van den Ende, R. G. H. Lammertink, and F. Mugele, *Phys. Rev. Lett.* **106**, 014501 (2011).
- [12] C. Monroe, L. Daikhin, M. Urbakh, and A. Kornyshev, *Phys. Rev. Lett.* **97**, 136102 (2006).
- [13] C. Decamps and J. De Coninck, *Langmuir* **16**, 10150 (2000).
- [14] M. Schneemilch, W. J. J. Welters, R. A. Hayes, and J. Ralston, *Langmuir* **16**, 2924 (2000).
- [15] P. Sen and C.-J. Kim, *Langmuir* **25**, 4302 (2009).
- [16] M. Paneru, C. Priest, R. Sedev, and J. Ralston, *J. Am. Chem. Soc.* **132**, 8301 (2010).
- [17] H. Li, M. Paneru, R. Sedev, and J. Ralston, *Langmuir* **29**, 2631 (2013).
- [18] J. Bird, S. Mandre, and H. Stone, *Phys. Rev. Lett.* **100**, 234501 (2008).
- [19] L. Chen, C. Li, N. F. van der Vegt, G. Auernhammer, and E. Bonaccorso, **Phys. Rev. Lett.** **110**, 026103 (2013).
- [20] R. Style, R. Boltyanskiy, Y. Che, J. Wettlaufer, L. A. Wilen, and E. Dufresne, *Phys. Rev. Lett.* **110**, 066103 (2013).
- [21] R. Pericet-Cámara, A. Best, H.-J. Butt, and E. Bonaccorso, *Langmuir* **24**, 10565 (2008).
- [22] R. Pericet-Cámara, G. K. Auernhammer, K. Koynov, S. Lorenzoni, R. Raiteri, and E. Bonaccorso, *Soft Matter* **5**, 3611 (2009).
- [23] E. R. Jerison, Y. Xu, L. A. Wilen, and E. R. Dufresne, *Phys. Rev. Lett.* **106**, 186103 (2011).
- [24] R. W. Style and E. R. Dufresne, *Soft Matter* **8**, 7177 (2012).
- [25] A. Marchand, S. Das, J. H. Snoeijer, and B. Andreotti, *Phys. Rev. Lett.* **109**, 236101 (2012).
- [26] L. A. Lubbers, J. H. Weijs, L. Botto, S. Das, B. Andreotti, and J. H. Snoeijer, *J. Fluid Mech.* **747**, R1 (2014).
- [27] M. E. R. Shanahan, *J. Phys. D: Appl. Phys.* **21**, 981 (1988).
- [28] M. E. R. Shanahan, *Langmuir* **10**, 1647 (1994).
- [29] A. Carre and M. E. R. Shanahan, *Langmuir* **11**, 24 (1995).
- [30] M. E. R. Shanahan and A. Carre, *Langmuir* **11**, 1396 (1995).

- [31] D. Long, A. Ajdari, and L. Leibler, *Langmuir* **12**, 5221 (1996).
- [32] A. Carre, J-C. Gastel and M. E. R. Shanahan, *Nature* **379**, 432 (1996).
- [33] M. C. Lopes and E. Bonaccorso, *Soft Matter* **8**, 7875 (2012).
- [34] M. C. Lopes and E. Bonaccorso, *Soft Matter* **9**, 7942 (2013).
- [35] See Supplemental Material
- [36] T. Ferreira and W. Rasband, ImageJ User Guide; <http://imagej.nih.gov/ij/>
- [37] Properly cured 10:1 Sylgard 184 film is usually considered as a rigid film in the literature. Here, we further establish the fact that such a film can be considered as a normal solid dielectric by showing that the electrowetting behaviour of a sessile, conductive droplet on the fabricated 10:1 Sylgard film conforms to the classical Lippmann-Young equation [1] (see the Supplemental Material).
- [38] J. Ralston, M. Popescu, and R. Sedev, *Annu. Rev. Mater. Res.* **38**, 23 (2008).
- [39] J. H. Snoeijer and B. Andreotti, *Annu. Rev. Fluid Mech.* **45**, 269 (2013).
- [40] J. Buehrle, S. Herminghaus, and F. Mugele, *Phys. Rev. Lett.* **91**, 086101 (2003).
- [41] J. Eggers and H. a. Stone, *J. Fluid Mech.* **505**, 309 (2004).
- [42] For contact line spreading velocity $\leq 10^{-4}$ m/s, the effect of viscous dissipation is usually negligible, and is routinely neglected compared to the viscoelastic energy dissipation (see refs. 28-30, 32). Here, the contact line velocity for electrospreeding on the softer dielectrics is $O(10^{-5} \text{ m/s})$, and hence the viscous dissipation can be neglected compared to the viscoelastic dissipation without any loss of generality.
- [43] A. Marchand, S. Das, J. H. Snoeijer, and B. Andreotti, *Phys. Rev. Lett.* **108**, 094301 (2012).